Journal of Solid State Chemistry 183 (2010) 2490–2495

Contents lists available at ScienceDirect

Journal of Solid State Chemistry

journal homepage: www.elsevier.com/locate/jssc

One-step fabrication and characterization of silica-sheathed ITO nanowires

Hyoun Woo Kim [a,*], Hyo Sung Kim [a], Han Gil Na [a], Ju Chan Yang [a], Rino Choi [a], Jae Kyeong Jeong [a], Chongmu Lee [a], Doo Young Kim [b]

[a] Division of Materials Science and Engineering, Inha University, Incheon 402-751, Republic of Korea
[b] Department of Chemistry, Michigan State University, East Lansing, MI 48824, USA

ARTICLE INFO

Article history:
Received 2 June 2010
Received in revised form
5 August 2010
Accepted 7 August 2010
Available online 19 August 2010

Keywords:
ITO
Nanowires
Silica
Photoluminescence
Growth mechanism

ABSTRACT

Novel $In_{1.94}Sn_{0.06}O_3$ (ITO)/amorphous SiO_x core–shell structures were successfully synthesized by simple thermal evaporation. Studies indicated that the core–shell structures typically consisted of a core of crystalline, ITO nanowires surrounded by a shell of amorphous, SiO_x tubular structures. We proposed a gold-catalyzed, vapor–liquid–solid process as the dominant mechanism for the growth of the core ITO nanowires, whereas SiO_x was grown in a tubular structure by a simultaneous and dynamic process. The possible reason for the preferential formation of the SiO_x shells on the outside of the core–shell structures, is discussed. In regard to the core/shell structures, three emission peaks of 2.73, 3.06, and 1.65 eV were observed in the room-temperature photoluminescence measurements, and were attributed to the SiO_x shell.

1. Introduction

Tin-doped indium oxide (ITO) has been widely used in a variety of fields, including gas sensors [1], photovoltaic cells [2], electrochromic devices [3], liquid crystal displays [4], and optoelectronic devices [5]. In particular, ITO is a wide band gap semiconductor (E_g=3.5 eV) and is therefore useful as a 'window layer' to allow light to penetrate the base semiconductor material [6]. On the other hand, one-dimensional (1D) nanomaterials have extraordinary physical and chemical properties in comparison to bulk materials. Their finite size confines the electron wave functions, resulting in quantized energy levels and a significant modification of the transport and optical properties.

As the most well-known and widely used transparent conducting oxide (TCO) material, ITO has a variety of current applications, which will be enhanced by the formation of ITO nanowires [7]. The 1D morphology is expected to enhance the field emission properties, which will facilitate the application of such nanowires in future field emission displays. The ITO nanowires support potential applications in electronic nanodevices due to the well-known metallic conductivity of ITO [8]. In addition, they have a higher surface-to-volume ratio, resulting in the higher-sensitivity of the ITO-based gas sensors.

In order to enhance the functionality of nanowires and protect against contamination, radial heterostructured nanowires have been created [9]. In particular, the coating of nanostructures with silica (SiO_x) in the form of amorphous inorganic polymer offers numerous advantages [10–12], including insulating characteristics, protection from contamination, mechanical and radiation damage, and chemical stability for preventing their aggregation in liquid. The SiO_x coating offers the possibility of integration with conventional integrated circuits and fabrication equipment. Moreover, the SiO_x surface can be easily functionalized with various coupling reagents, thereby facilitating the robust attachment of a variety of specific ligands [13,14]. For biorelated applications, the amorphous SiO_x demonstrates low toxicity even in systems that do not respond well to its crystalline form [15]. The SiO_x coating layer does not degrade the intrinsic optical properties of core materials owing to its optical transparency f or the visible absorption/emission [13,16]. The dielectric shells around the semiconductor core nanowires promise to enable the realization of surround-gate nanowire field-effect transistors [17].

In the present study, crystalline ITO nanowires surrounded with an amorphous SiO_x shell were successfully fabricated. The ITO nanowires sheathed with an outer tubular structure of insulating SiO_x will be useful for the interconnection in fabricating nanoelectronic nanodevices. For dye-sensitized solar cells, the long-term stability and conversion efficiency of ITO nanowires used as electrodes can be increased by coating them with a dense and stable insulating layer such as SiO_x [18]. Furthermore, ITO–silica-semiconductor or ITO–silica-metal structures can be fabricated by forming an additional shell on the core–shell structures, which will support promising applications in future nanosystems.

Owing to their importance, numerous researchers have fabricated 1D materials surrounded by a SiO_x shell, resulting in

* Corresponding author. Fax: +82 32 862 5546.
E-mail address: hwkim@inha.ac.kr (H.W. Kim).

0022-4596/$ - see front matter © 2010 Elsevier Inc. All rights reserved.
doi:10.1016/j.jssc.2010.08.012

a variety of systems such as Ge/SiO_x [19], TiO/SiO_x [11], MgO/SiO_x [20], and carbon nanotubes/SiO_x [21]. To the best of our knowledge, this is the first report on the preparation of an ITO/SiO_x core–shell structure. Furthermore, most of the previous fabrication procedures utilized two-step processes, in which the shell layer was subsequently deposited on the core nanowires, or one-step processes with a mixture of powders including the Si source. In the present paper, however, we fabricated the SiO_x-coated ITO nanowires via a simple, one-step heating process by using the Si substrate as the silica source. This approach will provide an inexpensive and simple scheme to support the application in future, ultra-large-scale integration devices. In addition, we suggest a growth mechanism for the core–shell structures. In the presence of gold (Au)-related tip nanoparticles, the catalytic role of Au is illuminated.

2. Experimental

The ITO/silica core–shell nanostructures were synthesized in a 51 mm inner-diameter quartz tube by means of directly heating a mixture of ITO and graphite powders (volume ratio=1:1). The ITO powders were prepared by grinding a ceramic target with a composition of $(In_2O_3)_{0.9}(SnO_2)_{0.1}$. The high purity ITO powders were placed in an alumina boat, which was located in the middle of the quartz tube. A piece of the Si wafer coated with a 3-nm Au layer was placed at the top of the alumina boat, which acted as a substrate for collecting the products. The Au layer on the Si substrate was deposited by ion sputtering (Emitech, K757X). The vertical distance between the source powders and the Au-coated substrate was approximately 7 mm.

Prior to the growth process, the tube was pumped to a base pressure of 150 mTorr. The substrate temperature was elevated from 25 °C at a rate of 10 °C min^{-1}. During the growth process, the substrate temperature was maintained at 950–1050 °C in a flow of argon (Ar) and oxygen (O_2) gas. To optimize the growth condition of the core–shell structures, the substrate temperature was varied in the range 950–1050 °C. The O_2 partial pressure was set to 3% in the Ar/O_2 carrier gas with a constant total pressure of 2 Torr. After 1 h of typical growth process, the substrate was cooled and removed from the furnace for characterization.

The as-synthesized product was examined by X-ray diffraction (XRD; Philips X'pert MRD diffractometer), scanning electron microscopy (SEM, Hitachi S-4300 SE), transmission electron microscopy (TEM), selected area diffraction (SAD), and energy-dispersive X-ray spectroscopy (EDX, using an EDAX spectroscope attached to TEM). Photoluminescence (PL) spectroscopy was conducted at room temperature with the 325 nm line from a He–Cd laser (Kimon, 1 K, Japan).

3. Results and discussion

Fig. 1a and b shows top-view SEM images of the samples at growth temperatures of 950 and 1050 °C, respectively. Fig. 1a revealed the film-like structure of the 950 °C-grown product. However, close examination revealed the films to comprise of space and cluster-like structures. In Fig. 1b, the 1050 °C-grown product exhibited 1D structures with a diameter in the range 60–220 nm. The associated diameter distribution is shown in the inset of Fig. 1b. The average diameter of the core–shell wires was estimated to be about 113 nm.

Fig. 2a shows an XRD pattern of the 950 °C-grown sample. Apart from weak peaks of the tetragonal rutile SnO_2 phase with lattice parameters of a=4.7382 Å and c=3.1871 Å (JCPDS File No. 46-1211), the most recognizable reflection peaks could

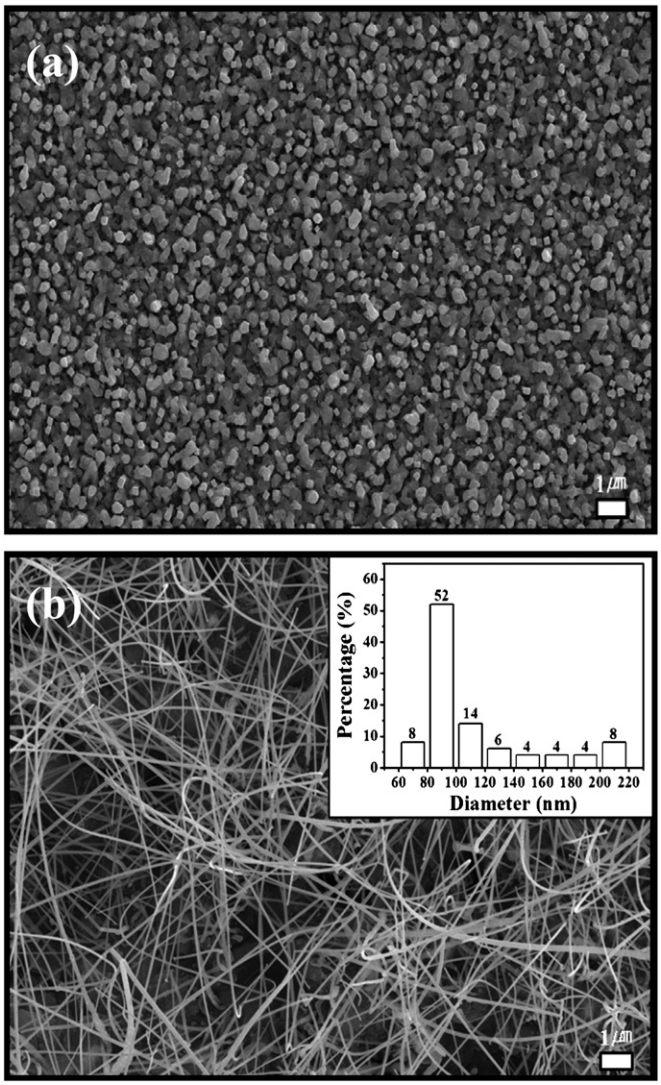

Fig. 1. Top-view SEM images of the samples at a growth temperature of (a) 950 and (b) 1050 °C (inset: corresponding diameter distribution).

be indexed to the diffraction peak in regard to the cubic $(In_{1.94}Sn_{0.06})O_3$ phase with a lattice parameter of a=10.1234 Å (JCPDS File No. 89-4596). On the other hand, Fig. 2b shows an XRD pattern of the 1050 °C-grown sample. The absence of any clear reflection peak beyond the noise level is suggestive of an overall amorphous structure for the 1050 °C-grown sample. However, close examination indicates the existence of very weak peaks corresponding to the (332), (440), (611), and (820) reflections of a cubic $(In_{1.94}Sn_{0.06})O_3$ phase. In addition, it is noteworthy that there are very weak peaks corresponding to the (101) and (200) reflections of a tetragonal rutile SnO_2 phase.

The low magnification TEM image of a nanowire shown in Fig. 3a reveals a two-segmented nanowire structure: a core and two coating layers (on both sides). Not only does the core structure have a straight-line morphology, but also the outer solid layer is relatively smooth and continuous along the nanowire. From Fig. 3a, the diameter of the core structure and the thickness of each shell layer were estimated to be 22 nm and about 72 nm, respectively.

Fig. 3b shows the corresponding SAD pattern, containing diffraction spots corresponding to the $\{0\bar{2}0\}$ and $\{\bar{1}\bar{2}0\}$ lattice planes of the tetragonal rutile SnO_2 phase (JCPDS File No. 46-1211). Another set of diffraction spots coincide with the {321},

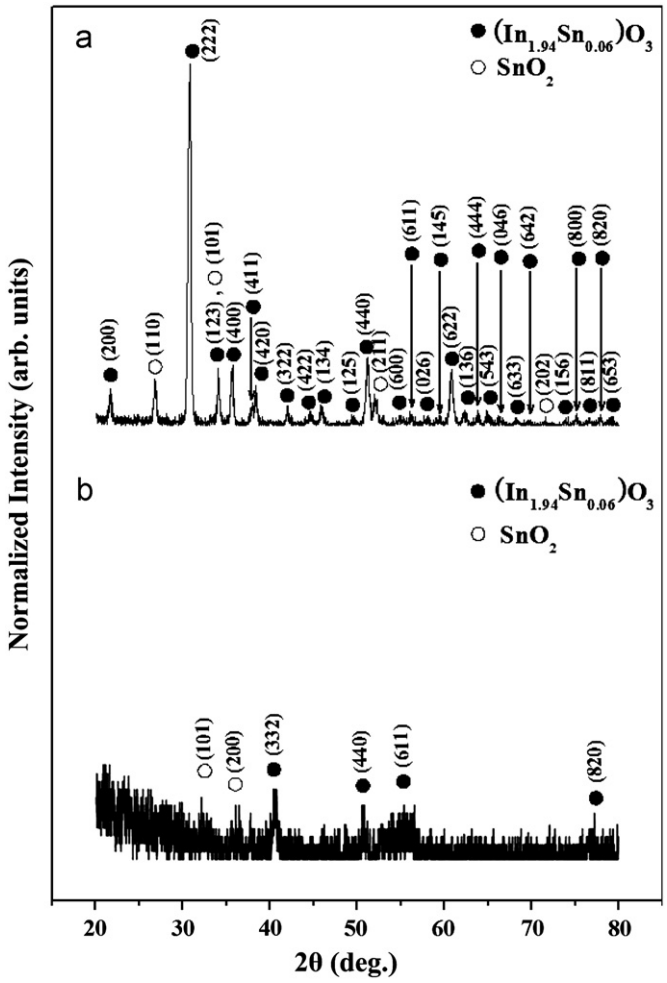

Fig. 2. XRD pattern of the samples at a growth temperature of (a) 950 and (b) 1050 °C.

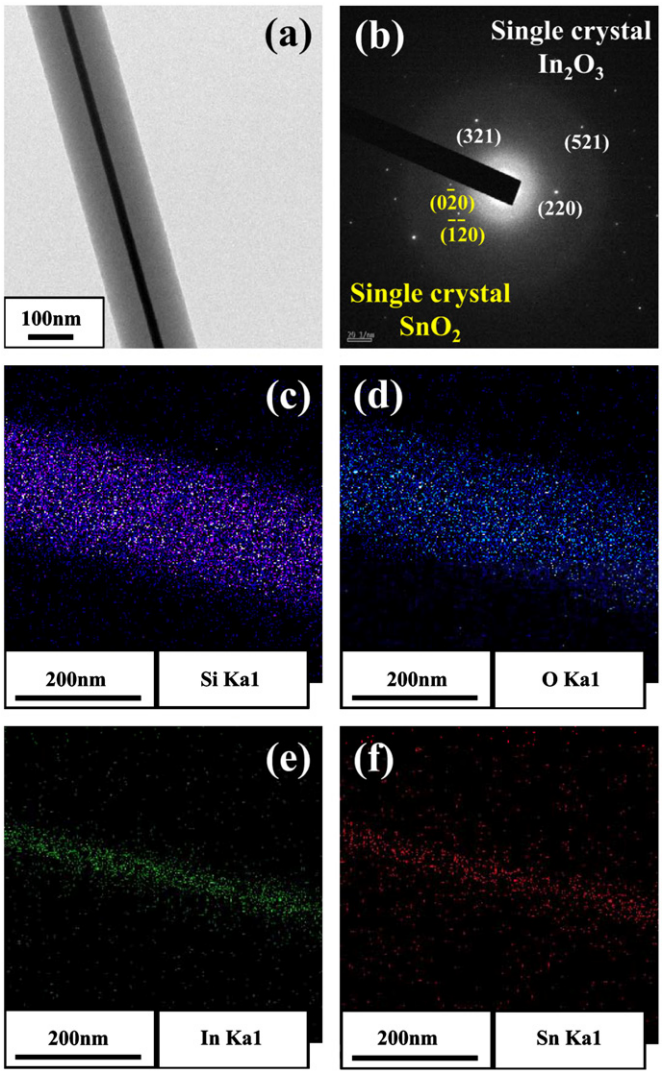

Fig. 3. (a) TEM image of a nanowire, and (b) corresponding SAD pattern. EDX elemental maps from a typical nanowire of (c) Si, (d) O, (e) In, and (f) Sn elements.

{521}, and {220} planes of the cubic bixbyite In_2O_3 structure with a lattice parameter of $a=10.118$ Å (JCPDS: 06-0416). In addition, the pattern shows a halo, presumably representing the amorphous SiO_x shell. Fig. 3c, d, e, and f shows the EDX elemental maps of Si, O, In, and Sn, respectively, for a typical 1D core–shell structure. The In and Sn atoms were concentrated in the core part of the 1D structure, whereas the Si and O atoms were found in the shell region. Accordingly, the EDX investigation revealed that the shell was comprised of Si and O elements. The presence of $In_{1.94}Sn_{0.06}O_3$ phase, also revealed in the XRD data (Fig. 2b), suggested that the core nanowires were mainly comprised of this phase.

Based on the above observations, we speculated on the growth mechanism of the core–shell structures. Since the TEM investigations indicated that the shell had a uniform thickness along the wire length, we discarded the possibility that the SiO_x shell was grown by the direct adsorption of SiO_x species from the gas phase. For the same reason, it is unlikely that the silica species originating from the substrate moved up the sides of the growing nanowire. Furthermore, observation of several TEM images revealed that the thickness of the shell layer varied in the range 60–120 nm, indicating significant variation in shell thickness among different wires. Therefore, it is unlikely that the core–shell nanowires were formed via a sequential process, in which the core nanowires form first and are subsequently uniformly coated with SiO_x shell layers [15]. Instead, we considered that the growth proceeded by the diffusion through the alloy particles to form the core nanowire and the migration of SiO_x on the surface of the alloy particle to the nanowire interface in a simultaneous and dynamic growth process. Similarly, Moore et al. [15] proposed the growth model of ZnS/SiO core–shell nanowires, in which the ZnS core was formed by volume diffusion across the catalyst particles while the silica shell was formed by surface diffusion on the catalyst particle.

Accordingly, we carried out a TEM investigation for closer examination of the tip region. Fig. 4a shows a low-magnification TEM image taken from the tip region of a typical core–shell structure. Fig. 4b shows an enlarged TEM image, revealing that the core part was comprised of a dark nanoparticle (indicated by an arrowhead). Fig. 4c shows an EDX spectrum taken from the region [A] in Fig. 4a, which represents the stem part of the core nanowire. Not only Si and O signals, but also Sn and In signals were observed. Cu and C signals originated from the microgrid mesh supporting the nanowires. The Si and O signals are attributed to the silica shell surrounding the core nanowire. Fig. 4d shows an EDX spectrum from the end region of the core–shell structure (region [B]), revealing that only Si and O elements were present on the ends of the core–shell structures. SEM investigation revealed that the end region of most core–shell

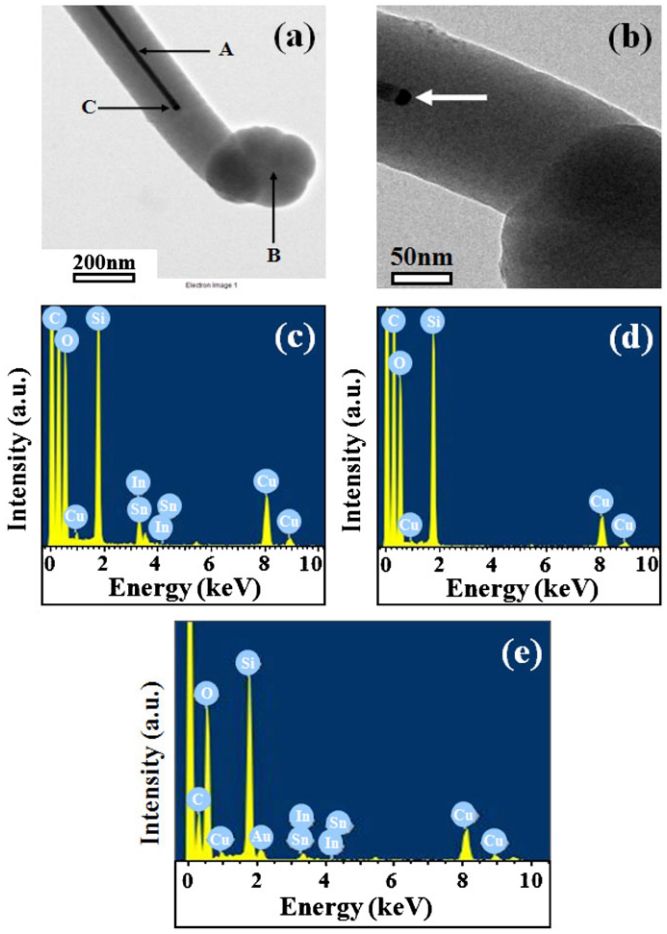

Fig. 4. (a) TEM image of an end region of a 1050 °C-grown 1D structure. (b) Enlarged TEM image for a tip part of a core nanowire. TEM-EDX spectra taken from the area indicated by arrows (c) A, (d) B, and (e) C in (a).

structures was comprised of agglomerated structures (see Supplementary Material S-1). According to Fig. 4d, the end region of the core–shell structure was mainly silica. Fig. 4e shows an EDX spectrum of the tip part of the core nanowire (region [C]), confirming the presence of elemental Au, in addition to Si, O, In, and Sn elements. This confirmed the core nanostructures to be ITO nanowires having Au-associated nanoparticles at the tip, whose growth was dominated by a vapor–liquid–solid (VLS) process. SEM investigations also supported that the 1D structures were rooted from the substrates (see Supplementary Material S-2).

Herein, we propose a possible growth model for the ITO/SiO_x core–shell structures, with Fig. 5 illustrating the associated process. At a sufficiently high temperature, the eutectic reaction between the Au thin layer and the Si substrate occurred firstly at 370 °C as the Au–Si eutectic alloys were formed (Fig. 5a) [22]. As the source powders were heated, the ITO-related vapors were generated and transferred to the Au-coated Si substrate. The ITO-related vapor was adsorbed onto the existing Si–Au alloy droplets, forming the In–Sn–Si–Au–O liquid (or solid) alloy. We conducted the same experiments using bare Si substrates without using the Au layer. No 1D structure was evident in the SEM investigation, indicating that the Au layer played a crucial role in the fabrication of the wires (see Supplementary Material S-3). Since the Si elements were not intentionally provided in the present study, the Si substrate must have been the main source of Si atoms. Despite the presence of several oxygen sources in the present

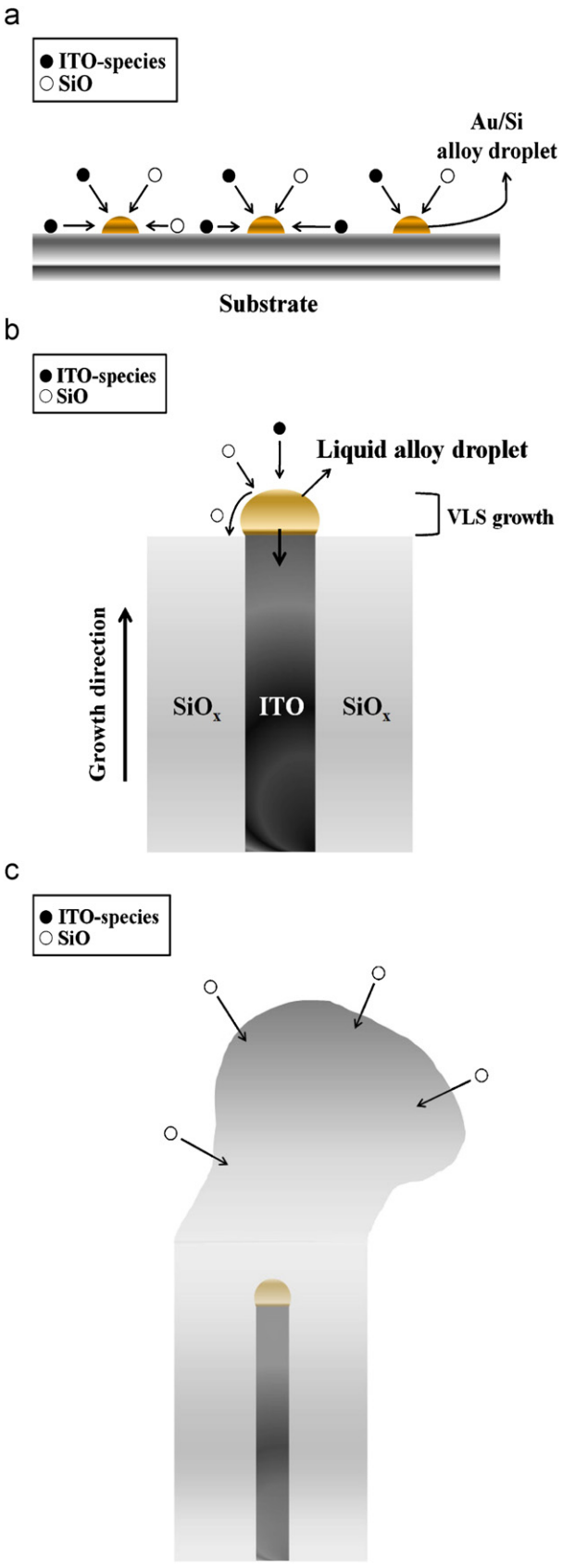

Fig. 5. Schematic illustration of a possible growth mechanism: (a) the initial stage, in which the Au–Si liquid droplet is formed, (b) the middle stage, in which core ITO nanowires are grown continuously, whereas SiO_x is grown in a tubular structure by a simultaneous and dynamic process, and (c) the final stage, in which the end structure is formed.

experiments, including residual oxygen in the chamber, leakage of the low vacuum system, and native oxide oxygen on the wafer surface, the main source must have been oxygen in the carrier gas. Since the temperature was sufficiently high (1050 °C) to induce the formation of 1D structures, whereas no thin 1D structure has been obtained at 950 °C (Fig. 1a), we surmise that the diffusion-induced suppression of 2D layer or cluster growth between nanowire seeds is a necessary condition for the formation of well-separated 1D structures (Fig. 5a).

At supersaturated concentrations, with the ITO-related vapor being constantly absorbed in the droplets, ITO then started to nucleate, which induced the growth of the core nanowires. At the same time, Si oxide was preferably precipitated on the solid ITO nanowires surface and formed the amorphous outer sheath (Fig. 5b). We considered the substrate temperature to be high enough to allow the phase separation into ITO and SiO_x. Although SiO_x commonly appears as a shell or tubular structure, and frequently forms coating layers over the growth products, it is not yet clear why the SiO_x separates out continuously to form the shell, with the ITO core filling the inside of shell.

Nevertheless, we propose two possible mechanisms for the formation of the SiO_x shell. The first is that Si atoms from the underlying Si substrate diffuse into the liquid alloy droplet, ultimately forming the SiO_x shell layer. However, this mechanism cannot explain why SiO_x separates out continuously to form the outer shell. Furthermore, it cannot help to attain the uniform shell thickness. The second possibility is that Si atoms react to form the volatile SiO vapor. We suggest that the formation of gaseous SiO will occur by the following reactions: $2Si(s)+O_2(g)\rightarrow 2SiO(g)$ [23]; $Si(s)+SiO_2(g)\rightarrow 2SiO(g)$ [24]. During the growth process, SiO and ITO-related vapors (In, Sn, ITO, etc.) are continuously absorbed into the liquid droplets. During the dynamic growth process, the ITO-related vapors are incorporated and diffuse through the Au-associated droplets to form the core ITO nanowires. At the same time, the gaseous SiO is adsorbed onto and travels on the droplet surface to the nanowire interface [15]. It is not clear when and how the SiO vapor is solidified into the SiO_x sheath. However, we surmise that the SiO vapor is barely soluble in the liquid droplet for some unknown reason. Liang et al. [25] postulated that the SiO vapor is barely soluble in liquid In. Accordingly, we suppose that the In-comprising liquid droplet in our present study prevented the SiO vapor from being incorporated into the droplet. Instead, the SiO vapor was dissociated or oxidized in the course of the surface diffusion process, ultimately forming the solid SiO_x sheath. In the final stage of the fabrication process, the growth of ITO core nanowires was retarded and ultimately stopped, whereas the SiO_x shell grew continuously, resulting in the formation of an irregularly shaped, SiO_x structure (Fig. 5c).

Fig. 6 and its inset show the PL emission spectra of the SiO_x-coated ITO nanowires grown at 1050 and at 950 °C, respectively. The broad emission spectra of the 1050 °C-grown sample can be divided into three Gaussian functions, centered at 2.73, 3.06, and 1.65 eV. The PL emission spectrum from the 1050 °C-grown sample is typical of that usually observed from the SiO_x nanowires [26]. The bands at around 2.73 and 3.06 eV can be ascribed to the neutral oxygen vacancy and to the twofold coordinated silicon lone-pair centers, respectively [27,28]. In addition, the red emission in silica was related to the nonbridging oxygen hole centers [27,29,30].

On the other hand, the broad emission spectrum of the 950 °C-grown sample contained a 2.15 eV-peaked emission band, with a very weak additional peak at around 2.66 eV. Luminescence bands at an energy of 2.0–2.5 eV have been reported in ITO structures [11,18,31], which are known to be mainly related to the surface defect states. Although further detailed study is necessary, it is possible that the weak peak at 2.66 eV was ascribed to either the SiO_x phase or the ITO phase. In addition, the 2.66 eV-peak in the blue region can be attributed to the SnO_2 phase. Similarly, previous study revealed that the SnO_2 phase exhibited the blue emission [32].

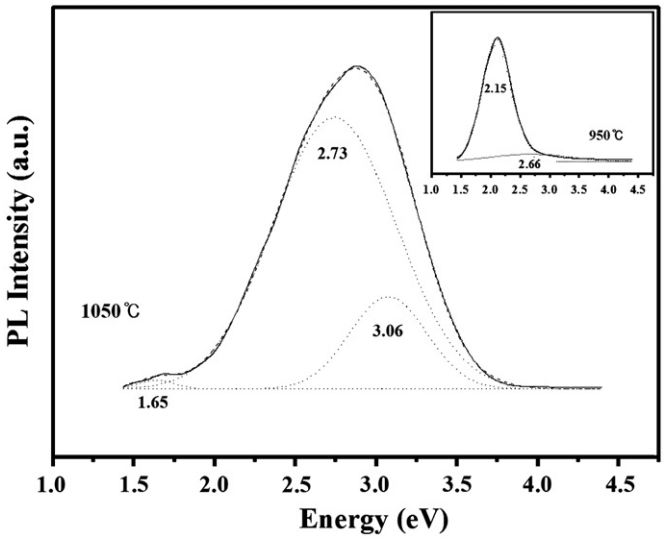

Fig. 6. Room-temperature PL spectrum excited by 325 nm light for the SiO_x-coated ITO nanowires grown at 1050 °C (inset: corresponding PL spectrum for the 950 °C-grown sample).

Although not shown here (see Supplementary Material S-4), the overall intensity of the PL spectrum was significantly reduced by increasing the growth temperature from 950 to 1050 °C and, in particular, the 2.15 eV-peaked emission band was completely suppressed. This result was ascribed to the shielding effect of the SiO_x sheath, by which the ITO core nanowires make a negligible contribution to the emission of the wires. In addition, the surface defect states on the ITO nanowires, which are the origin of the 2.15 eV-peaked emission, may have become ineffective via the surface-coating of SiO_x shell layer. We are presently conducting further systematic investigation to elucidate the detailed mechanisms of the PL emission.

4. Conclusions

Novel ITO/amorphous SiO_x core–shell 1D structures were synthesized by the simple heating of ITO powders. Their morphology, microstructures, and optical properties were characterized by SEM, TEM, EDX, and PL. These studies indicated that the product typically consisted of a core of crystalline, $In_{1.94}Sn_{0.06}O_3$ nanowires and a shell of amorphous, SiO_x tubular structures. Due to the presence of Au-related nanoparticles at the tip, we proposed an Au-catalyzed, VLS process as the dominant mechanism for the growth of the core ITO nanowires. Also, we discussed the possible growth mechanism which explained the preferential formation of the SiO_x shells on the outside of the core–shell structures. Room-temperature PL measurements of the core/shell nanostructures exhibit three emission peaks of 2.73, 3.06, and 1.65 eV, being attributed to the SiO_x shell. The insulating nature of the SiO_x sheaths will create a perfect electrical isolation of the ITO cores, supporting the proposed application of the prepared nanowires in nanoelectronic devices.

Acknowledgments

This research was supported by National Nuclear R&D Program through the National Research Foundation of Korea (NRF) funded

by the Ministry of Education, Science and Technology (2010-0017556).

Appendix A. Supplementary materials

Supplementary data associated with this article can be found in the online version at doi:10.1016/j.jssc.2010.08.012.

References

[1] X.Y. Xue, Y.J. Chen, Y.G. Liu, S.L. Shi, Y.G. Wang, T.H. Wang, Appl. Phys. Lett. 88 (2006) 201907.
[2] J.R. Bellingham, A.P. Mackenize, W.A. Philips, Appl. Phys. Lett. 58 (1991) 2506.
[3] V. Teixeira, H.N. Cui, L.J. Meng, E. Fortunato, R. Martins, Thin Solid Films 420 (2002) 70–75.
[4] K. Osaza, T. Ye, Y. Aoyagi, Thin Solid Films 246 (1994) 58–64.
[5] I. Hambergend, C.G. Granquist, J. Appl. Phys. 60 (1986) R123–R159.
[6] A. Salehi, Thin Solid Films 324 (1998) 214–218.
[7] S.J. Limmer, S.V. Cruz, G.Z. Cao, Appl. Phys. A 79 (2004) 421–424.
[8] D.M. Mattox, Thin Solid Films 204 (1991) 25–32.
[9] L.J. Lauhon, M.S. Gudiksen, C.L. Wang, C.M. Lieber, Nature 420 (2002) 57–61.
[10] Y. Zhang, K. Suenage, C. Colliex, S. Iijima, Science 281 (1998) 973–975.
[11] Y.B. Li, Y. Bando, D. Golberg, Y. Uemura, Appl. Phys. Lett. 83 (2003) 3999–4001.
[12] Y. Wang, Z. Tang, X. Liang, L.M. Liz-Marzan, N.A. Kotov, Nano Lett. 4 (2004) 225–231.
[13] A. Schroedter, H. Weller, R. Eritja, W.E. Ford, J.M. Wessels, Nano Lett. 2 (2002) 1363–1367.
[14] M. Bruchez Jr., M. Moronne, P. Gin, S. Weiss, A.P. Alivisatos, Science 281 (1998) 2013–2016.
[15] D. Moore, J.R. Morber, R.L. Snyder, Z.L. Wang, J. Phys. Chem. B 112 (2008) 2895–2903.
[16] A. Pan, S. Wang, R. Liu, C. Li, B. Zou, Small 1 (2005) 1058–1062.
[17] E. Sutter, F. Camino, P. Sutter, Appl. Phys. Lett. 94 (2009) 083109.
[18] K.P. Kalyanikutty, G. Gundiah, C. Edem, A. Govindaraj, C.N.R. Rao, Chem. Phys. Lett. 408 (2005) 389–394.
[19] X.-M. Meng, J.-Q. Hu, Y. Jiang, C.-S. Lee, S.-T. Lee, Appl. Phys. Lett. 83 (2003) 2241–2243.
[20] H.W. Kim, J.W. Lee, C. Lee, M.A. Kebede, Polym. Adv. Technol. 20 (2009) 246–250.
[21] H.W. Kim, S.H. Shim, J.W. Lee, Carbon 45 (2007) 2695–2698.
[22] T. Adachi, Surf. Sci. 506 (2002) 305–312.
[23] D. Starodub, E.P. Gusev, E. Garfunkel, T. Gustafsson, Surf. Rev. Lett. 6 (1999) 45–52.
[24] B. Geng, G. Meng, L. Zhang, G. Wang, X. Peng, Chem. Commun. 20 (2003) 2572–2573.
[25] C. Liang, Y. Shimizu, T. Sasaki, H. Umehara, N. Koshizaki, J. Mater. Chem. 14 (2004) 248–252.
[26] H.W. Kim, H.S. Kim, M.A. Kebede, H.G. Na, J.C. Yang, Y.S. Koo, J.H. Jung, N.J. Hur, Appl. Surf. Sci. 255 (2009) 8425–8429.
[27] H. Nishikawa, T. Shitoyama, R. Nakamura, Y. Ohki, K. Nagasawa, Y. Hama, Phys. Rev. B 45 (1992) 586–591.
[28] M. Kohketsu, K. Awazu, H. Kawazoe, M. Yamane, Jpn. J. Appl. Phys. 28 (1989) 615–621.
[29] L.N. Skuja, A.R. Silin, Phys. Status Solidi (a) 56 (1979) K11–K13.
[30] S. Munekuni, T. Yamanaka, Y. Shimogaichi, R. Tohmon, Y. Ohki, K. Nagasawa, Y. Hama, J. Appl. Phys. 68 (1990) 1212–1217.
[31] Q. Wan, Z.T. Song, S.L. Feng, T.H. Wang, Appl. Phys. Lett. 85 (2004) 4759–4761.
[32] D. Maestre, A. Cremades, J. Piqueras, J. Appl. Phys. 95 (2004) 3027–3030.